

# Effect of diffusible hydrogen level on heat-affected zone hydrogen-induced cracking of high-strength steels

Xin Yue · Xiu-Li Feng · John C. Lippold

Received: 29 April 2013 / Accepted: 15 July 2013 / Published online: 28 August 2013  
© International Institute of Welding 2013

**Abstract** The implant test was used to investigate the heat-affected zone (HAZ) hydrogen-induced cracking (HIC) sensitivity of two high-strength naval steels, HY-100 and HSLA-100. Welding was performed using the gas-metal arc welding process, and a high and a low hydrogen level was introduced using an Ar-15% $H_2$  and an Ar-5% $H_2$  shielding gas, respectively. The lower critical stress for HIC at the two hydrogen levels was determined using the implant test. In both cases, failure occurred in the coarse-grained HAZ (CGHAZ). The microstructures of the CGHAZ of the two steels were characterized by means of both optical and transmission electron microscopy, and Vickers hardness measurements. The fracture behavior was studied using scanning electron microscopy. Both the implant test results and the fractographic analysis indicate that HSLA-100 has better resistance to HAZ cracking and better tolerance to higher hydrogen contents than HY-100. This is attributed to the presence of a mixed martensitic/bainitic microstructure in the HSLA-100 CGHAZ, relative to a fully martensitic CGHAZ with higher hardness in HY-100.

**Keywords** Heat-affected zone · Hydrogen embrittlement · Implant tests · Fractography · High-strength steels

## 1 Introduction

High-strength steels are the principal structural materials in naval hull construction nowadays, and this will continue to be the trend in the foreseeable future, as a result of their good combination of high strength and low-temperature toughness.

Of all the high-strength naval steels, HY-100 and HSLA-100 are still widely used today [1, 2].

HY-100 was developed in order to meet the requirement for high-strength applications in naval construction. The high strength and toughness of HY-100 steels is a result of the tempered martensitic microstructure. Alloying elements such as Cr, Mo, and Ni are added to increase the hardenability of this steel. The heat treatment to develop the tempered martensite microstructure first requires heating the steel to a temperature above  $A_{C3}$ , where it is in the austenite region, and then rapidly quenching to form untempered martensite. The as-quenched martensite has high strength and hardness but low toughness, and it is susceptible to hydrogen-induced cracking. Therefore, after quenching, a tempering process in the range of 550 to 650 °C is employed to form tempered martensite, which has an optimal combination of strength and toughness [3, 4].

HSLA-100 was developed after HY-100, in order to reduce fabrication costs. A combination of alloy content and thermo-mechanical controlled processing (TMCP) technology is used to achieve excellent properties through microstructural control. HSLA-100 has very low carbon content (less than 0.1 wt.%) and less than 5 wt.% total alloy content (Mn, Mo, Cu, Ni, and Nb). Very fine grain size in the range of 5 to 10  $\mu\text{m}$  can be obtained in HSLA-100 through TMCP. The microstructure of HSLA-100 consists of a mixture of martensite and lower bainite. In addition to the fine grain size and the martensite/lower bainite microstructure, various carbides, nitrides, carbonitrides, and/or  $\epsilon$ -copper precipitates are finely dispersed in the matrix and provide additional strengthening without compromising toughness [5–8].

It has been found that welds in high-strength steels are often susceptible to HIC, particularly in the heat-affected zone (HAZ) where a combination of high hardness, residual stress, and the presence of hydrogen can lead to cracking [9–12]. The mechanism of HIC has been extensively studied and many

X. Yue (✉) · X.-L. Feng · J. C. Lippold  
Welding Engineering Program, The Ohio State University, 1248  
Arthur E. Adams Drive, Columbus, OH 43221, USA  
e-mail: yuexinosu@gmail.com

theories have been proposed, including the surface adsorption theory by Petch [13], the decohesion theory by Troiano [14], and the slip softening model proposed by Beachem [15]. Even though a unified mechanism for HIC still does not exist, it is generally agreed that the occurrence of HIC in the HAZ of high-strength steels requires the simultaneous presence of a threshold level of hydrogen, a susceptible microstructure (usually martensite) and tensile residual stress [16]. The formation of hard and brittle martensite in HAZ is very common as a result of the high hardenability of high-strength steels, and high residual stress usually cannot be avoided in the weld joint due to the fabrication process. Therefore, high-strength steels having a good tolerance to higher hydrogen levels are desired from a practical welding standpoint since the welding requirements (preheat, interpass, and postweld heat treatment controls) can be relaxed. As a result, for current high-strength naval steels, determining the susceptibility to HIC as a function of hydrogen level is of critical importance.

In the present study, the cracking sensitivity at high and low hydrogen levels for HY-100 and HSLA-100 steels was evaluated using the implant test. The coarse-grained HAZ (CGHAZ) microstructure was characterized using both optical and transmission electron microscopy, and fracture behavior was studied by scanning electron microscopy. The research results contribute to a weldability database for naval steels, which can be used as a benchmark for developing new high-performance steels.

## 2 Materials and experimental procedures

HY-100 and HSLA-100 were provided in the form of 12.7 mm (0.5 in.) rolled plate by the Naval Surface Warfare Center, Carderock Division, West Bethesda, MD, USA. Table 1 lists the chemical composition of the two steels evaluated in this investigation. The base metal microstructures of the two steels are shown in Fig. 1. The 0.2 % yield strength and ultimate tensile strength of HY-100 was measured to be 737 and 799 MPa, respectively. For HSLA-100, the 0.2 % yield strength and ultimate tensile strength were measured to be 765 and 880 MPa, respectively. The implant specimens were machined from the steel plate along the rolling direction, with dimensions shown in Table 2. The implant test, which was originally developed by Henri Granjon [17], is used in the present investigation to evaluate the HAZ HIC susceptibility. This test method has been used extensively for investigating hydrogen cracking in the HAZ, due to the fact that the stress, hydrogen level, and microstructure can be independently varied and controlled [18–20].

The details of the implant test are shown in Fig. 2a–d. The 0.5-in. (12.7 mm)-long 10-32 UNF thread was inserted into the clearance hole in the center of the specimen plate, with the top surface of the thread flush with the specimen plate surface. A weld bead was deposited using the gas metal arc welding process with 0.047-in. (1.2 mm) SuperArc® LA-100 wire

**Table 1** Chemical composition (weight percent) of HY-100 and HSLA-100

Element (wt.%)	HSLA-100	HY-100
C	0.051	0.18
Mn	0.90	0.28
Si	0.25	0.21
P	0.008	0.008
S	0.002	0.002
Cu	1.17	0.15
Ni	1.58	2.32
Cr	0.60	1.37
Mo	0.37	0.26
V	<0.01	<0.01
Nb	0.017	<0.01
Ti	<0.01	<0.01

(AWS: ER100S-G) on the surface of the specimen plate directly over the 10-32 UNF thread and the hole. Welding parameters used are as follows: voltage, 30 V; current, 215–225 A; and travel speed, 12 in./min (5.1 mm/s). This corresponds to an average heat input of 33 kJ/in. (1.3 kJ/mm). Same welding parameters were used for all the welding runs. A HAZ was created in the 10-32 thread region after welding, with the 10-32 thread used to generate stress concentration and cause cracking to occur in the HAZ instead of the fusion zone. Ar+15%H<sub>2</sub> or Ar+5%H<sub>2</sub> shielding gas at a flow rate of 45 ft<sup>3</sup>/h (21.2 L/min) was used in order to introduce a high and a low diffusible hydrogen level into the weld pool, respectively. The diffusible

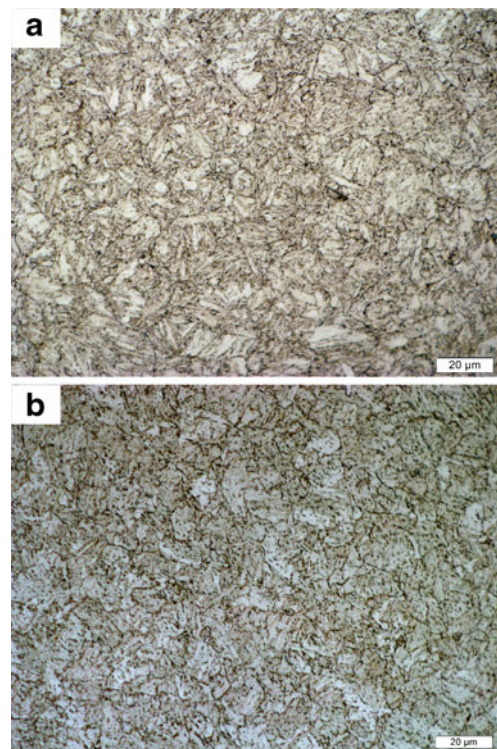


**Fig. 1** Base metal microstructure. **a** HY-100, **b** HSLA-100

**Table 2** Specimen plate/implant specimen dimensions

Specimen plate	
Material	A36 steel
Plate thickness, in. (mm)	0.5 (12.7)
Plate width, in. (mm)	2 (50.8)
Plate length, in. (mm)	4 (101.6)
Length of test bead, in. (mm)	3.5 (88.9)
Hole diameter, in. (mm)	0.201 (5.1)
Implant specimen	
Material	HY-100, HSLA-100
Total length of implant specimen, in. (mm)	1 (25.4)
Type of thread	10-32 UNF
Pitch, in. (mm)	1/32 (0.79)
Major diameter, in. (mm)	0.1900 (4.83)
Minor diameter, in. (mm)	0.1517 (3.85)
Thread length, in. (mm)	0.5 (12.7)
Thread angle	60°
Thread root radius, in. (mm)	0.004 (0.1)

hydrogen content was measured to be 10.5 mL/100 g when using Ar+15% $H_2$  gas and 6.5 mL/100 g using Ar+5% $H_2$  gas, by means of the gas chromatograph method in accordance with AWS A4.3.

Two minutes after the completion of welding, the implant sample was subject to a static tensile stress. The implant sample was free of bending, torsion, or shock loading as a result of the

specific design of the implant testing system (OSU Modified Implant Test System, OSU-MITS). Details of the test procedure have been reported elsewhere [21]. The time required for the implant specimen to fail under a given stress level was recorded by the data acquisition system integrated with the OSU-MITS, and a tensile stress–time to failure relationship was obtained for each steel. The highest stress at which no failure occurs after 24-h loading was defined as the lower critical stress (LCS) [22], which was taken as an index to determine susceptibility to HIC.

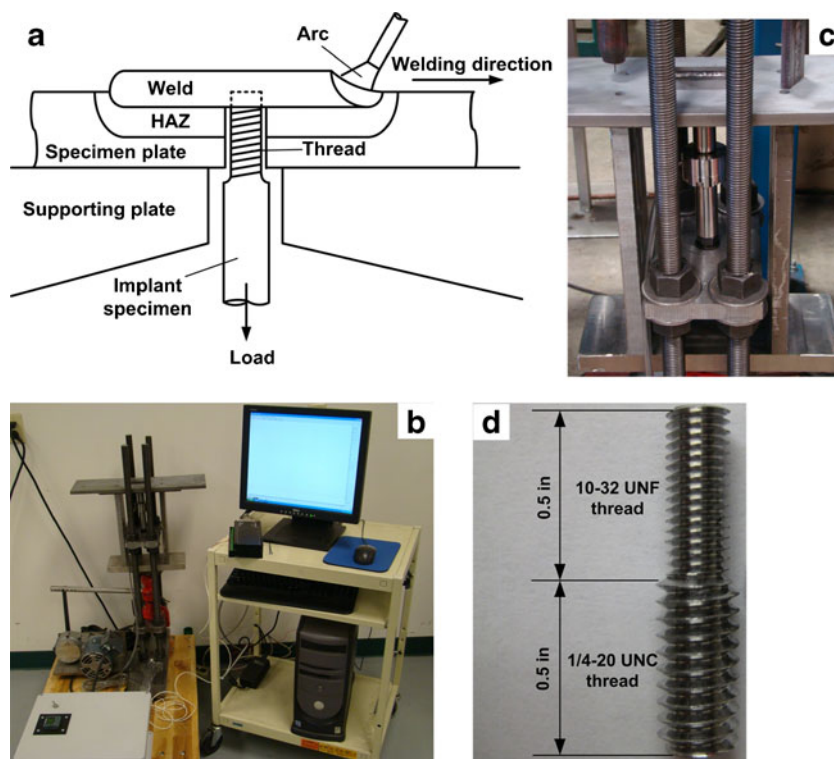
Metallographic samples were sectioned perpendicular to the welding direction along the axis of the implant specimens. Then they were mounted, ground, polished, and etched with 5 % nital and examined using optical microscopy. A Helios 600 (FEI Co., Hillsboro, OR) dual beam focused ion beam was used for extracting and thinning samples for transmission electron microscopy (TEM) analysis. The TEM foils were evaluated in a Philips CM200 TEM operated at 200 kV. The fracture surface of the implant samples was examined using a Philips XL30F ESEM. Vickers hardness measurements were conducted along the axis of the implant specimens using a 1 kg load, in accordance with ASTM E 384-10.

### 3 Results and discussion

#### 3.1 Weld macrostructure

Figure 3a shows the macrostructure of a typical test weld sectioned along the axis of the implant specimen. A distinct

**Fig. 2** The OSU-MITS and implant specimen. **a** Schematic drawing of the implant test, **b** full view of the OSU-MITS, **c** close-up view showing an implant specimen under loading and an unloaded one on the top right corner, **d** the implant specimen



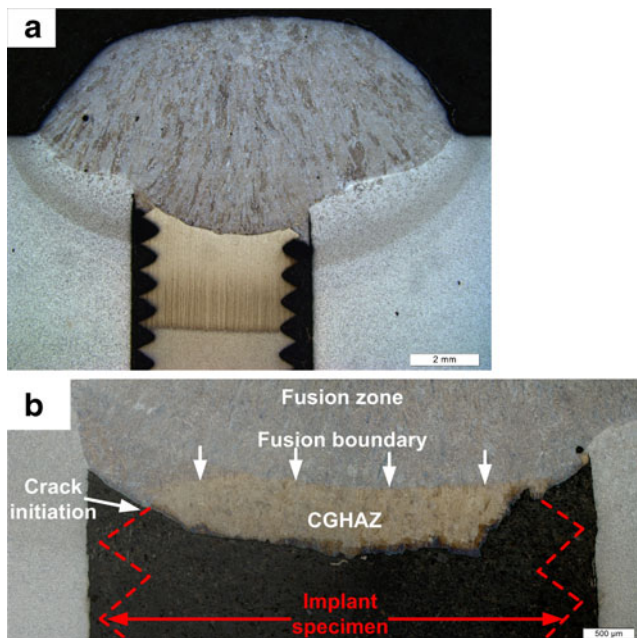


**Fig. 3** a Representative weld macrostructure, b macrostructure of a typical fractured joint after loading showing the fracture path

HAZ was created along the axis of sample and the threads provide the stress concentration that allows cracking in the most susceptible region. Some isolated porosity can be observed in the fusion zone, since the hydrogen added through the shielding gas does not have sufficient time to escape from the weld pool. The width of HAZ in the implant specimen is wider than that in the adjacent specimen plate due to its smaller mass and shallower temperature gradient relative to the adjacent specimen plate.

Two minutes after welding is completed, the implant specimen is subjected to a static tensile load. The macrostructure of a representative fractured weld is shown in Fig. 3b, from which the fracture path can be clearly seen. As shown in Fig. 3b, the fusion boundary separating the fusion zone and the CGHAZ is indicated by the white arrows. The red dotted line delineates the original profile of the implant specimen before loading. It can be seen that the hydrogen cracking initiates from the thread root closest to the fusion boundary in the CGHAZ and propagates approximately 0.3–0.4 mm away from the fusion boundary. As has been seen previously, the CGHAZ is the most HIC susceptible region, due to the presence of a coarse prior austenite grain size and high-hardness microstructure [7, 12, 23].

### 3.2 The implant test results with two hydrogen levels

Figure 4a, b shows the implant test results for HY-100 welded with Ar+5% $H_2$  and Ar+15% $H_2$  shielding gas, respectively.

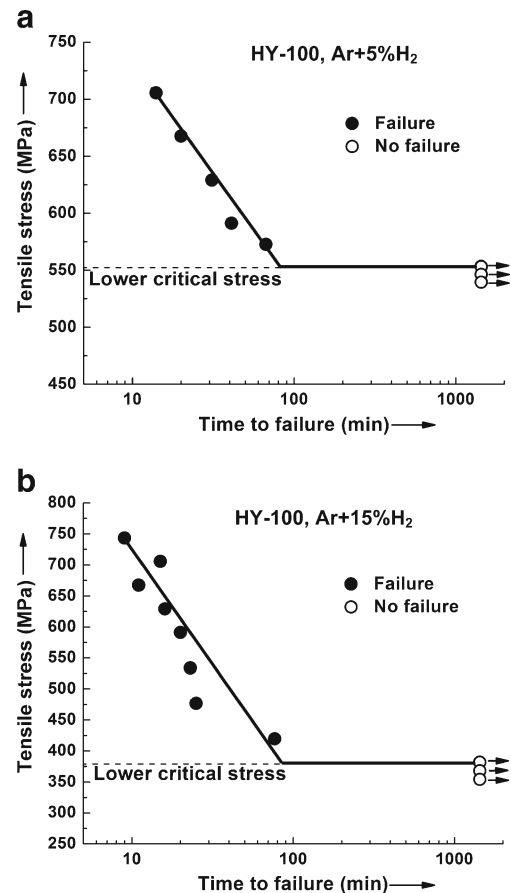


**Fig. 4** The implant test curves of HY-100: a welded with Ar+5% $H_2$ , b welded with Ar+15% $H_2$

When the hydrogen level is 6.5 mL/100 g, as shown in Fig. 4a, the LCS was determined to be 551 MPa. However, it drops dramatically to 379 MPa if 10.5 mL/100 g diffusible hydrogen was introduced to the weld pool, as shown in Fig. 4b.

For HSLA-100, at the low hydrogen level, the LCS was determined to be 723 MPa, as shown in Fig. 5a. And it only slightly decreases to 703 MPa when the high level of hydrogen was introduced to the weld pool, as shown in Fig. 5b. The drastic decrease in LCS for HY-100 in comparison to HSLA-100 indicates that HY-100 is more sensitive to hydrogen content than HSLA-100 and that HSLA-100 can tolerate more diffusible hydrogen without a significant reduction in HIC resistance. In addition, welded with the same hydrogen level, the LCS of HSLA-100 is much higher than that of HY-100, and at equivalent stress levels, the incubation time before fracture for HSLA-100 is longer as compared to HY-100. The implant test data clearly demonstrate that HSLA-100 has good resistance to HAZ hydrogen cracking and tolerance to higher hydrogen levels, both of which are desirable characteristics of high-strength steels used for welded fabrication under high restraint conditions.

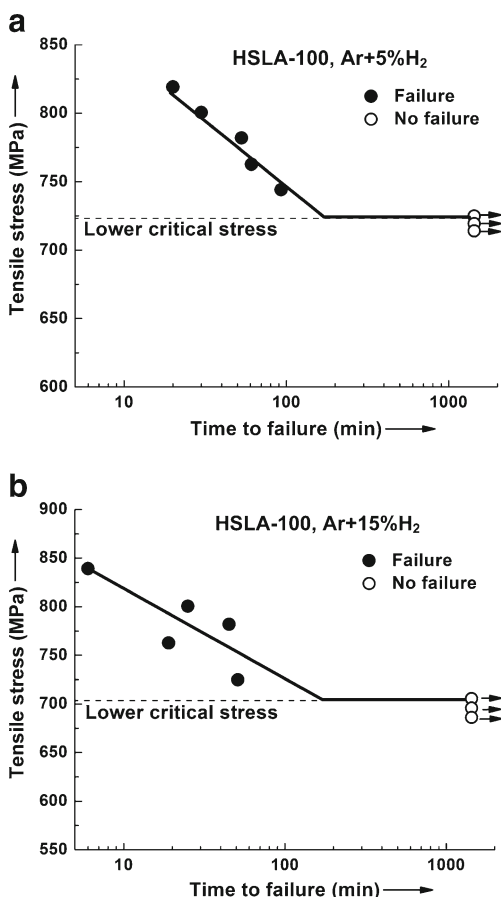


**Fig. 5** The implant test curves of HSLA-100: **a** welded with Ar+5% $H_2$ , **b** welded with Ar+15% $H_2$

### 3.3 Weld CGHAZ microstructure

Since it has been found that the CGHAZ is the most susceptible to HIC among the HAZ regions, the microstructure of this region was evaluated to determine the effect on hydrogen cracking sensitivity. Vickers hardness measurements were conducted, and the results are shown in Fig. 6. The CGHAZ microstructure of HY-100 and HSLA-100 were also characterized by means of optical microscopy and transmission electron microscopy, as shown in Figs. 7 and 8.

The hardness traverse is obtained along the axis of the implant specimens, starting in the fusion zone and running through the HAZ to the unaffected base metal. The region within the confines of the two black solid lines in Fig. 6a, b represents the HAZ, and the red dotted line is the approximate boundary separating the CGHAZ and the adjacent fine-grained HAZ. It can be seen in Fig. 6a, b that the HAZ hardens as a result of welding. From Fig. 6a, this hardness increase is especially remarkable for HY-100. The CGHAZ hardness is in the range of 440–464  $HV_{1.0}$ , much higher than 260–280  $HV_{1.0}$  of the fusion zone and the 280–300  $HV_{1.0}$  of the HY-100 base metal. It is shown in Fig. 6b that a hardness increase in HSLA-100 HAZ is also observed, although the increase is

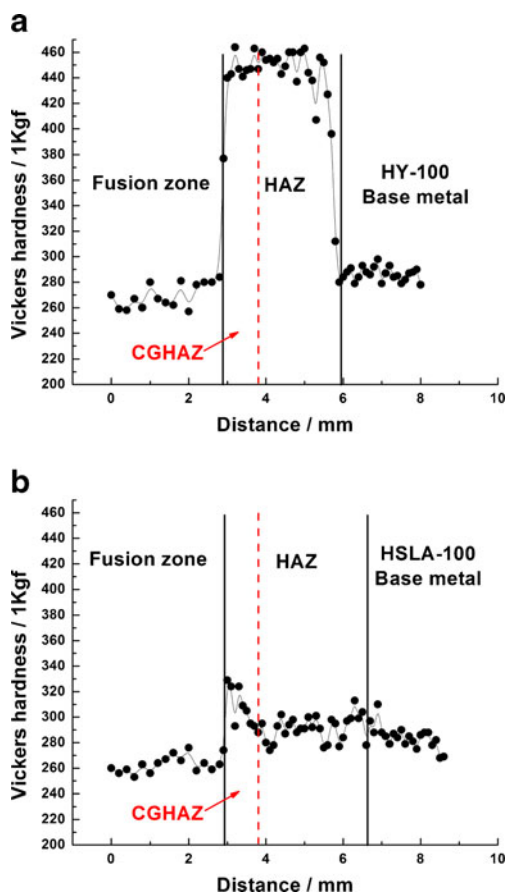


**Fig. 6** Vickers hardness measurements taken along the axis of the implant specimen. **a** HY-100, **b** HSLA-100

not as dramatic. The hardness of HSLA-100 CGHAZ is in the range of 293–329  $HV_{1.0}$ , only slightly higher than that of HSLA-100 base metal in the range of 280–300  $HV_{1.0}$ .

Based on microstructure analysis (Fig. 7a), it can be seen that the CGHAZ microstructure of HY-100 is fully martensitic; the martensite laths can be observed at higher magnification TEM bright-field micrograph, as shown in Fig. 7b. The martensite formed is therefore described as “lath” martensite, with an average Vickers hardness of 449  $HV_{1.0}$ .

For the CGHAZ microstructure of HSLA-100, besides the dark-etching martensite, long needle-like bainite nucleating from prior austenite grain boundaries can be observed, as shown in Fig. 8a. In the TEM micrograph shown in Fig. 8b, a group of martensite laths can be observed at the bottom left corner, and bainite laths can be seen at the top right part of the micrograph, with platelet-like cementite precipitating within the bainite laths. Those cementite precipitates are oriented at a preferential angle with the primary bainite lath growth direction, and this is the characteristic feature distinguishing lower bainite from upper bainite or lath martensite [24]. Thus, the CGHAZ microstructure of HSLA-100 contains a mixture of lath martensite and lower bainite, with an average Vickers hardness of 311  $HV_{1.0}$ . The formation of lower bainite and

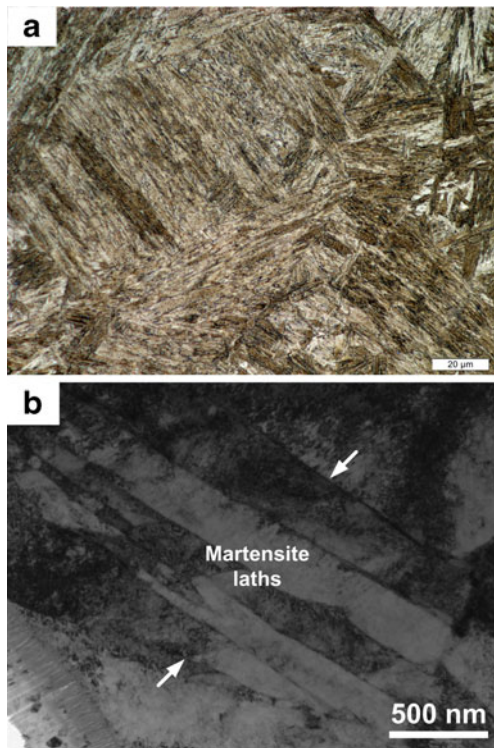


**Fig. 7** CGHAZ microstructure of HY-100. **a** Optical, **b** bright-field TEM

martensite in the HSLA-100 CGHAZ, in contrast to fully martensitic HY-100, results from the lower alloy content and

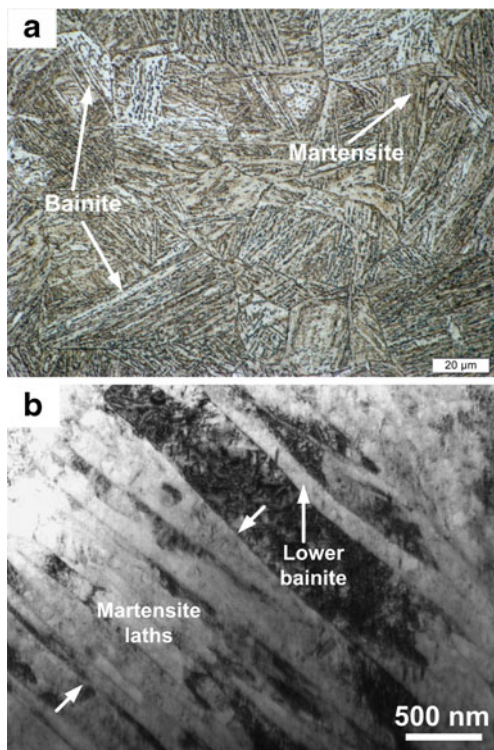


**Fig. 8** CGHAZ microstructure of HSLA-100. **a** Optical, **b** bright-field TEM

corresponding lower hardenability of HSLA-100 than HY-100, as indicated by the carbon equivalent, 0.62 for HSLA-100 and 0.75 for HY-100 [7]. The hardness of the CGHAZ of HSLA-100 is much lower as compared to HY-100 for two reasons. First, it contains lower-hardness bainite, and second, the hardness of martensite which is determined by carbon content is much lower in HSLA-100 (0.051 wt.%) than HY-100 (0.18 wt.%).

### 3.4 Fracture behavior

The fracture behavior of HY-100 and HSLA-100 under the two diffusible hydrogen levels has been investigated by SEM, as shown in Figs. 9, 10, 11, 12. The fracture morphology of HY-100 welded with Ar+5% $H_2$  is shown in Fig. 9a–d. Figure 9a shows the general fracture appearance. Based on morphology, the fracture surface can be roughly divided into three regions (designated I, II, and III). As shown in Fig. 9b, region I is predominantly intergranular (IG) failure, which constitutes the bulk of the fracture surface. Region III exhibits a microvoid coalescence (MVC) fracture mode. Quasi-cleavage (QC) was observed in region II, which is the transition between regions I and III.

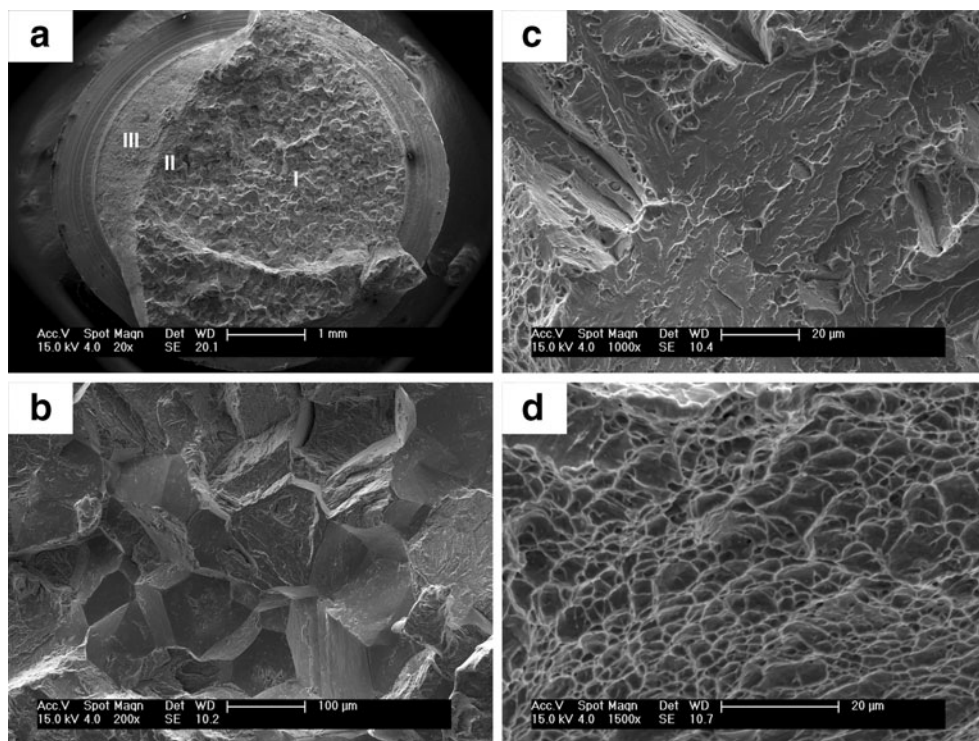
When welded with Ar+15% $H_2$ , the fracture morphology of HY-100 is shown in Fig. 10a–d. Similar to the fracture behavior with Ar+5% $H_2$ , the failure mode of regions I, II, and III is IG, QC, and MVC, respectively. However, it should be noted that when lower diffusible hydrogen level is present, the area of the faceted IG failure on the fracture surface decreases and the QC and MVC are increased, as seen by comparing Figs. 9 and 10.

The fracture morphology of HSLA-100 welded with Ar+5% $H_2$  is shown in Fig. 11a–d. As shown in Fig. 11a, the fracture surface of HSLA-100 exhibits considerably more ductility as compared to HY-100. Small areas of faceted IG failure can be observed in region I on the fracture surface, and QC and MVC was found in region II and III, respectively. Region III with the MVC failure mode constitutes the majority of the fracture surface.

The fracture morphology of HSLA-100 specimens with higher diffusible hydrogen levels is shown in Fig. 12a–d. Similar to the fracture surface with low hydrogen, the IG failure mode is only observed in the area a few grain diameters away from the thread root. The QC mode is adjacent to region I, and the area of region II does not change significantly relative to the low hydrogen level. The area of region III with MVC failure mode is slightly decreased as compared to that with low hydrogen level.

The fracture morphology is a good indicator of the HAZ HIC cracking sensitivity to hydrogen of the two steels. At both high and low hydrogen levels, IG failure is predominant on the HY-100 fracture surface. The fracture surface of HSLA-100 is more ductile with MVC as the dominant failure mode. As shown in Figs. 4 and 5, the fracture morphology reinforces

**Fig. 9** Fracture morphology of HY-100 implant specimen welded with Ar+5%H<sub>2</sub>. **a** General fracture appearance, **b** region I, IG; **c** region II, QC; **d** region III, MVC



the fact that HSLA-100 has better resistance to HAZ cracking than HY-100. The better resistance of HSLA-100 to HIC is a result of the formation of lower hardness microstructure of martensite and lower bainite in CGHAZ.

For HY-100, higher diffusible hydrogen level leads to an increase in the area of IG and decrease in the area of QC and MVC. This is a good indication that HY-100 is sensitive to hydrogen content, which is also evidenced by the drastic

**Fig. 10** Fracture morphology of HY-100 implant specimen welded with Ar+15%H<sub>2</sub>. **a** General fracture appearance; **b** region I, IG; **c** region II, QC; **d** region III, MVC

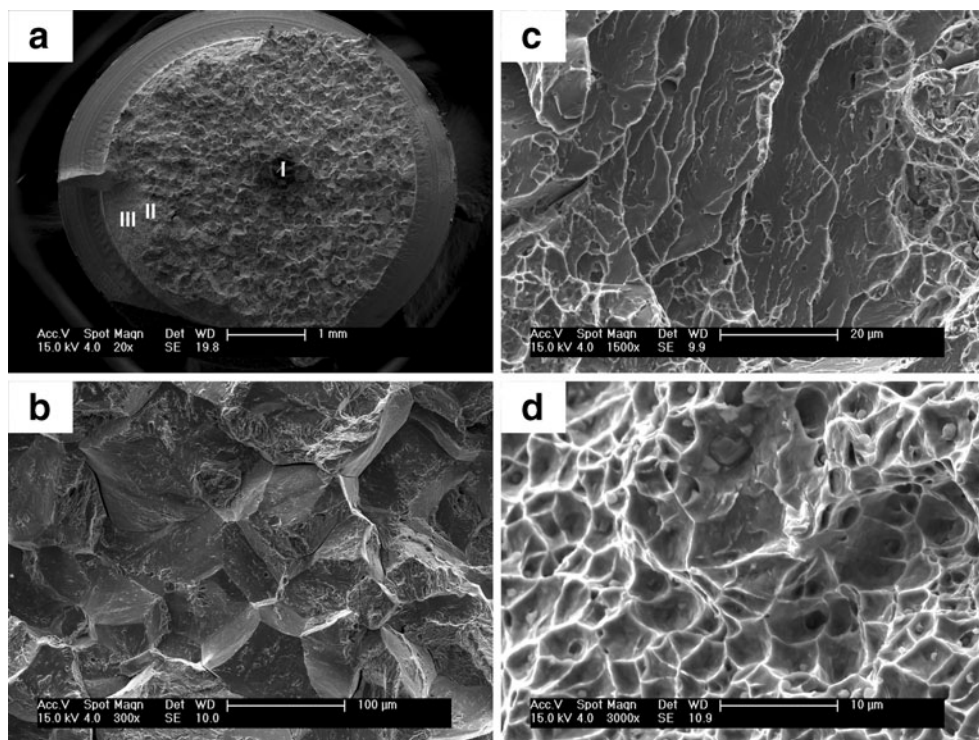
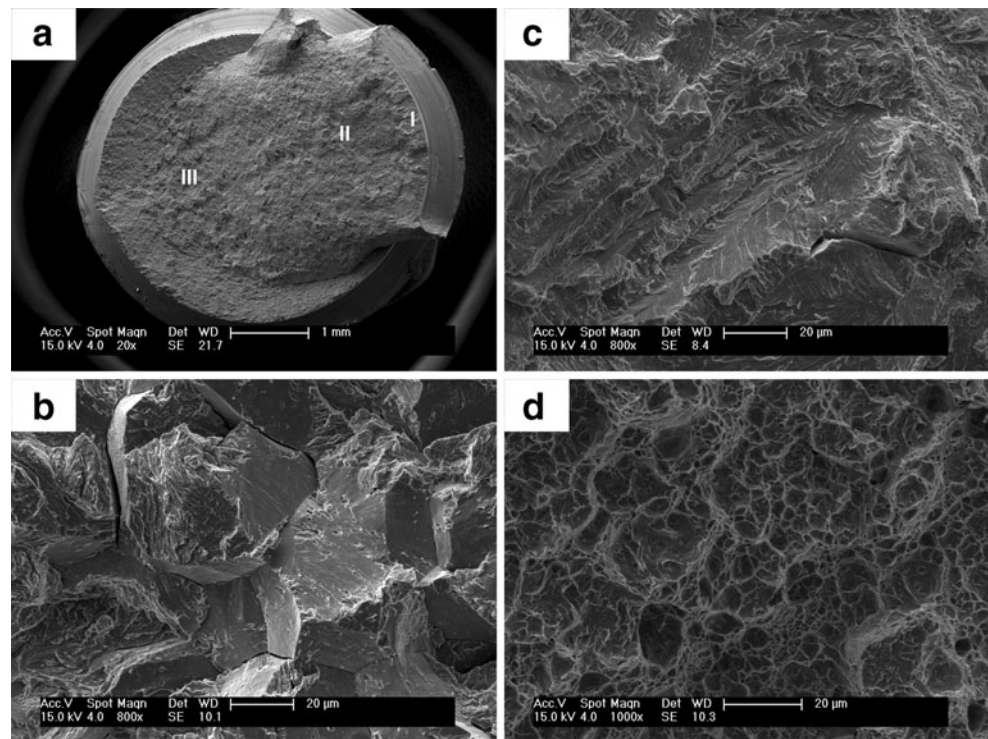


**Fig. 11** Fracture morphology of HSLA-100 implant specimen welded with Ar+5%H<sub>2</sub>. **a** General fracture appearance; **b** region I, IG; **c** region II, QC; **d** region III, MVC

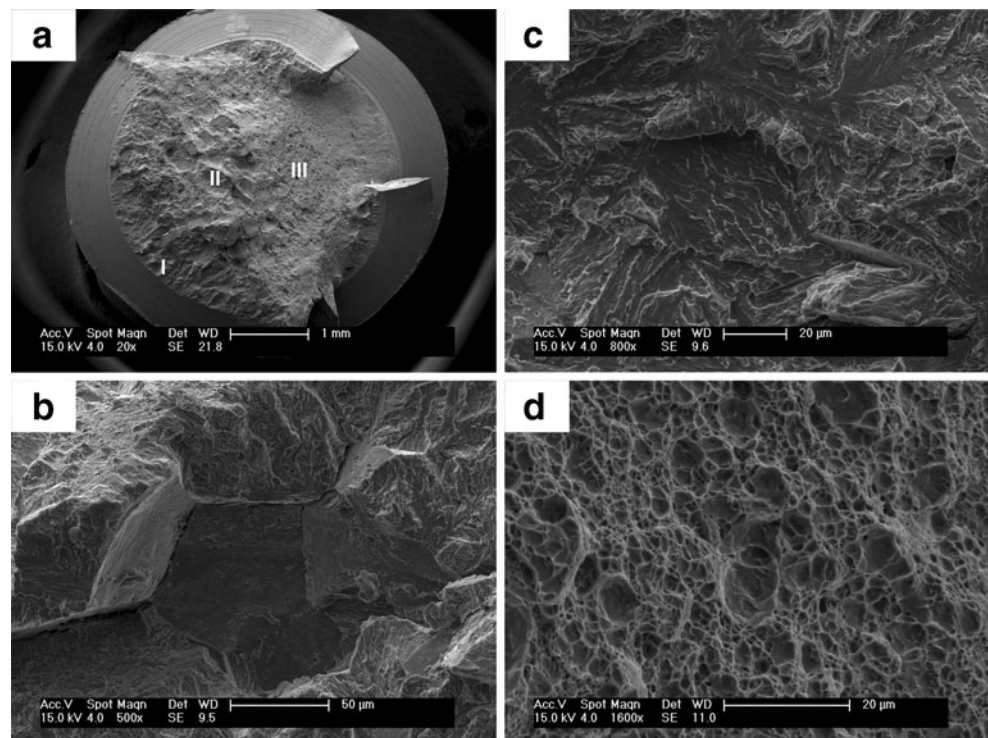


decrease of LCS from 551 MPa with low hydrogen to 379 MPa with high hydrogen level. The high sensitivity of HY-100 is because of its martensitic microstructure in CGHAZ with high hardness in the range of 440–464 HV<sub>1,0</sub>,

which allows crack initiation and propagation at much lower stresses (and stress intensities).

For HSLA-100, with the two hydrogen levels, MVC is observed to be the dominant failure mode on the fracture

**Fig. 12** Fracture morphology of HSLA-100 implant specimen welded with Ar+15%H<sub>2</sub>. **a** General fracture appearance; **b** region I, IG; **c** region II, QC; **d** region III, MVC





surface, and there is not an obvious difference of fracture morphology at the two diffusible hydrogen levels. The LCS only slightly decreases from 723 MPa with low hydrogen to 703 MPa with high hydrogen. Both these observations indicate that HSLA-100 has a strong tolerance to higher hydrogen level as to avoid HAZ HIC. This is attributed to the lower carbon content and low hardenability of HSLA-100, and the resultant formation of a lower hardness microstructure of martensite and lower bainite in the CGHAZ.

#### 4 Conclusions

1. From implant test results, the LCS for HY-100 decreases from 551 MPa with low hydrogen level of 6.5 mL/100 g to 379 MPa with high hydrogen level of 10.5 mL/100 g. For HSLA-100, the LCS only slightly decreases from 723 MPa with low hydrogen to 703 MPa with high hydrogen.
2. Both steels exhibit an increase in HAZ hardness as a result of the welding thermal cycle. The CGHAZ microstructure of HY-100 is predominantly martensite, with average hardness of 449 HV<sub>1.0</sub>. For HSLA-100, a mixture of martensite and lower bainite in the CGHAZ microstructure results in an average hardness of 311 HV<sub>1.0</sub>.
3. The formation of martensite in HY-100 CGHAZ results from its higher hardenability relative to HSLA-100. The higher CGHAZ hardness of HY-100 is due to a combination of a fully martensitic microstructure and higher carbon content (0.18 vs. 0.05 wt.%).
4. IG fracture is the predominant failure mode observed on HY-100 fracture surface at both hydrogen levels. The fracture surface of HSLA-100 exhibits little intergranular fracture and is generally dominated by MVC.
5. For HY-100, increasing the level of diffusible hydrogen results in an increase in the area of IG fracture and decrease in the area of QC and MVC. For HSLA-100, there is no obvious difference in fracture morphology with the two hydrogen levels.
6. Both the implant test results and the fracture behavior analysis indicate that, compared to HY-100, HSLA-100 has much better resistance to HAZ HIC and better tolerance to increases in hydrogen levels. This is attributed to the lower hardness and mixed martensite/lower bainite microstructure in the HSLA-100 CGHAZ.

**Acknowledgments** The authors gratefully acknowledge the financial support of the Office of Naval Research, award no. N000140811000, grant officers Dr. Julie Christodoulou and Dr. William Mullins. The authors would like to thank Johnnie DeLoach, Matthew Sinfield, and Jeffrey Farren with the Naval Surface Warfare Center Carderock Division, West Bethesda, MD for providing the HY-100 and HSLA-100 steels used in this study and for valuable discussions regarding the weldability of naval steels. Dejian Liu and Geoffrey Taber are acknowledged for their constructive ideas and assistance with building the implant testing system.

#### References

1. Czyryca EJ, Link RE, Wong RJ, Aylor DA, Montemarano TW, Gudas JP (1990) Development and certification of HSLA-100 steel for naval ship construction. *Nav Eng J* 102(3):63–82
2. Montemarano TW, Sack BP, Gudas JP, Vassilaros MG, Vanderveldt HH (1986) High strength low alloy steels in naval construction. *J Ship Prod* 2(3):145–162
3. Czyryca EJ (1993) Advances in high strength steel technology for naval hull construction. *Key Eng Mater* 84–85:491–520
4. Czyryca EJ, Vassilaros MG (1993) Advances in low carbon, high strength ferrous alloys. Research & Development Report by Naval Surface Warfare Center, Report No. CDNSWC/SME-92/64, April
5. Spanos G, Fonda RW, Vandermeer RA, Matuszeski A (1995) Microstructural changes in HSLA-100 steel thermally cycled to simulate the heat-affected zone during welding. *Metall Mater Trans A* 26:3277–3293
6. Liu S (1992) Metallography of HSLA steel weldments. *Key Eng Mater* 69–70:1–20
7. Yue X, Lippold JC, Alexandrov BT, Babu SS (2012) Continuous cooling transformation behavior in the CGHAZ of naval steels. *Weld J* 91(3):67s–75s
8. Shome M, Mohanty ON (2006) Continuous cooling transformation diagrams applicable to the heat-affected zone of HSLA-80 and HSLA-100 steels. *Metall Mater Trans A* 37:2159–2169
9. Yurioka N, Suzuki H (1990) Hydrogen assisted cracking in C-Mn and low alloy steel weldments. *Int Mater Rev* 35(4):217–249
10. Wongpanya P, Boellinghaus T, Lothongkum G (2006) Effects of hydrogen removal heat treatment on residual stresses in high strength structural steel welds. *Weld World* 50:96–103
11. Devletian JH, Fichtelberg ND (2001) Controlling hydrogen cracking in shipbuilding. *Weld J* 80(11):46–52
12. Yue X, Lippold JC (2013) Evaluation of heat-affected zone hydrogen induced cracking in Navy steels. *Weld J* 92(1):20s–28s
13. Petch NJ, Stables P (1952) Delayed fracture of metals under static load. *Nature* 169(4307):842–843
14. Troiano AR (1960) The role of hydrogen and other interstitials in the mechanical behavior of metals. *Trans Am Soc Met* 52:54–80
15. Beachem CD (1972) A new model for hydrogen-assisted cracking (Hydrogen "embrittlement"). *Metall Trans* 3:437–451
16. Kou S (2003) *Welding metallurgy*. John Wiley & Sons Inc, New Jersey, pp 410–417
17. Granjon H (1969) The implants method for studying the weldability of high strength steels. *Met Constr Br Weld J* 1(11):509–515
18. Kannengiesser T, Boellinghaus T (2013) Cold cracking tests—an overview of present technologies and applications. *Weld World* 57(1):3–37
19. Gedeon SA, Eagar TW (1990) Assessing hydrogen-assisted cracking fracture modes in high-strength steel weldments. *Weld J* 69(6):213s–220s
20. Signes EG, Howe P (1988) Hydrogen-assisted cracking in high-strength pipeline steels. *Weld J* 67(8):163s–170s
21. Yue X, Feng XL, Lippold JC (2013) Quantifying heat-affected zone hydrogen-induced cracking in high-strength naval steels. *Weld J* 92(9):265s–273s
22. AWS B4.0:2007. Standard methods for mechanical testing of welds. Am Weld Soc, pp 67–71
23. Nawrocki JG, DuPont JN, Robino CV, Marder AR (2001) The postweld heat treatment response of simulated coarse-grained heat-affected zones in a new ferritic steel. *Metall Mater Trans A* 32:2585–2594
24. Bhadeshia HKDH (2001) Bainite in steels: transformations, microstructure and properties. IOM Communications, London, pp 63–75